Journal of Alloys and Compounds, 194 (1993) 331–338
JALCOM 7204

Lattice destabilization and amorphization by mechanical alloying in the Ti–Al system*

E. Bonetti and G. Valdré
Dipartimento di Fisica, Università di Bologna, GNSM and Consorzio INFM, via Irnerio 46, I-40126 Bologna (Italy)

S. Enzo
Dipartimento di Chimica Fisica, Università di Venezia and Consorzio INFM, DD 2137, I-30123 Venezia (Italy)

G. Cocco
Dipartimento di Chimica, Università di Sassari, via Vienna 2, I-07100 Sassari (Italy)

(Received November 20, 1991; in final form March 18, 1992)

Abstract

Analytical electron microscopy and X-ray diffraction techniques have been used to study the amorphization process of the Ti–Al system induced by mechanical alloying. The results show that the entire transformation develops from the diffusion of Al into the Ti crystal lattice, beginning as soon as a well-developed layered structure is formed in the powders in the early milling stages (after 6 h). Collapse of the highly distorted host lattice occurs after milling for 20 h and gives rise to a homogeneous amorphous structure at 24 h. Further milling time (34 h) produces an f.c.c. nanocrystalline phase with a Ti–Al at. ratio of approximately 3 and with the lattice parameter $a = 0.42$ nm.

1. Introduction

In the past few years an increasing number of experimental approaches have been utilized to achieve metastable nanocrystalline and amorphous phases in metallic systems. These include several solid-state amorphizing transformations (SSAT) induced, *e.g.* by irradiation [1], low temperature interdiffusion reactions [2], annealing of bulk metastable phases [3] and mechanical alloying (MA) [4].

In particular, MA through ball milling of metal powders has proved to be a solid-state processing method that can be usefully employed to produce amorphous materials in amounts suitable for technological purposes [5]. The first report on amorphization by mechanical attrition of crystalline intermetallic compound of yttrium and cobalt was by Yermakov *et al.* in 1981 [6] and the first report on amorphization by solid-state reaction (SSR) of two pure crystalline metals was by Schwarz and Johnson in 1983 [7].

Following from these papers, it has been observed experimentally that MA of several elemental crystalline powders can result in the formation of amorphous phases whose chemical composition corresponds to that of the original powder mixture. Meanwhile a great effort has been made to understand the basic mechanisms of SSAT, when it derives from MA of pure elemental metal powders or the mechanical milling of crystalline intermetallic compounds. The ultimate purpose is to develop a consistent and general theory to describe the common features of all kinds of SSAT.

A local melting, arising from a temperature increase caused by powder particles trapped between colliding balls during milling, followed by rapid solidification, was proposed by Yermakov *et al.* [6] as a possible cause of amorphization. As pointed out by Schwartz *et al.* [5], during MA of pure metal powders, the powder particles attain a finely layered structure formed by alternating films of the original elements. This is a situation similar to that of thin metallic multilayers. In the above condition a strong diffusion of one atomic species is possible, aided by lattice defects created by plastic deformation. The enhanced diffusivity resulting from high dislocation density and localized heating may promote a close mixing of atoms, once the thickness of the layers is in the submicron range [8].

However, the theory of amorphization by enhanced solid state interdiffusion seems, at least in some systems,

*Paper presented at the Symposium on Solid State Amorphizing Transformations, TMS Fall Meeting, Cincinnati, OH, October 21–24, 1991.

0925-8388/93/$6.00

not to hold. This is the case, for example, in the non-fast diffusing system V–Zr [9]. Moreover, as observed by Schwarz and Koch [10], amorphization by ball milling (BM) may be reached in a binary alloy starting from the pure crystalline elements as well as from an equilibrium compound with the same composition. This last observation rules out the advanced hypothesis that a decrease in the free energy of the system may constitute a major driving force for amorphization.

Amorphization through SSR deriving from a breaching of an elastic stability limit with subsequent collapse of the crystalline structure was proposed by Johnson [11] and Fecht *et al.* [12].

In the case of intermetallic compounds submitted to irradiation, there is now experimental evidence that chemical disorder is the main driving force for the crystal to amorphous transformation. Okamoto *et al.* [13] have observed a clear connection in the Zr_3Al intermetallic between a critical irradiation dose and an elastic softening, indicative of an elastic instability directly related to a lattice dilatation, at the onset of amorphization. A theoretical analysis by molecular dynamics by Massobrio [14] in the $NiZr_2$ intermetallic has established a critical value for the long-range order parameter corresponding to a volume expansion of nearly 2%, which destroys the topological crystalline order.

Recently, in several mixtures of pure elemental metal powders submitted to MA and investigated by X-ray diffraction (XRD) techniques, Enzo *et al.* [15] have obtained experimental evidence indicative of the formation of highly distorted solid solutions and intermetallic compounds, collapsing at the onset of the crystal to amorphous transition.

In this paper a direct technique capable of high analytical resolution such as transmission electron microscopy (TEM) with a field emission gun (FEG) and equipped with a parallel electron energy loss spectrometer (PEELS) and an X-ray energy dispersive spectrometer (EDS), was employed to investigate in detail the structural transformation leading to BM amorphization. The observations were focused in particular on detecting unusual solid solution and lattice disorder effects induced by BM in the Ti–Al system, in which an amorphization reaction had previously been observed [16].

In addition, particular attention was paid to investigating the possible role of contaminants affecting the structural transformations.

2. Experimental details

Nominally pure Al and Ti crystalline powders (200 mesh, Alfa Products), were mixed in the appropriate 3Ti–1Al atomic ratio, and milled for selected times, at room temperature in a WC vial with a Spex-mixer/mill model 8000. The weight of the mixed powders was about 10 g and the ball to powder weight ratio was 8:1. The milling was conducted in an Ar atmosphere, to minimize oxygen contamination.

Powder diffraction patterns have been obtained by an automated θ:2θ diffractometer according to the procedure described in detail elsewhere [17].

Specimens for TEM observation were prepared according to two different procedures. In the first, specimens were obtained by retrieving the powders, which are transparent to the electron beam on their edge, on perforated carbon grids or adhesive coated grids. The second procedure utilizes an ultramicrotome to prepare thin electron transparent slices (about 80 nm thick) from a dispersion of powder particles embedded in epoxydic resin.

Observations have been performed with an FEG Philips EM 400T electron microscope, operating at 120 kV. EDS analyses have been carried out by means of an EDAX PV 9900 X-ray EDS, while PEELS readings were accomplished by means of GATAN 606 magnetic sector, coupled to a three quadrupole-YAG-CCD parallel acquisition system developed at the Cavendish Lab., Cambridge (UK) [18].

3. Results

3.1 X-ray diffraction

Some relevant results on the system under investigation obtained by XRD are shown in Fig. 1, which illustrates the spectra evolution at successively increasing milling times, reported as logarithm of intensity *vs.* the scattering vector $\mathbf{q}=(4\pi \sin \theta/\lambda)$ in the range 23–33 nm^{-1}.

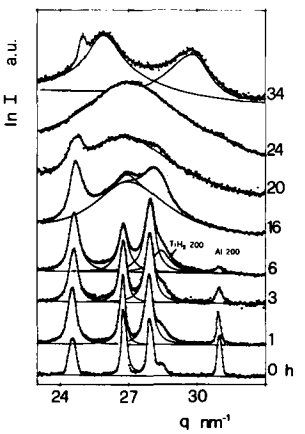

Fig. 1. XRD patterns of Ti_{75}–Al_{25} powders as a function of milling time, from bottom to top. Note the dissolution of Al in the α-Ti lattice at the early stages of milling. The amorphous phase is well developed at milling for 24 h.

The pattern at the bottom refers to the mixture of the h.c.p. Ti and f.c.c. Al, before milling. The first peak at 24.50 nm^{-1} is identified as Ti(010), while the second one at 26.9 nm^{-1} is the superposition of the Ti(002) and Al(111) contributions. The third peak at 28.05 nm^{-1} belongs to Ti(011) and its shoulder in the right side is assigned to TiH_2 (200) in agreement with neutron diffraction observations on CuTi alloys prepared by BM with the same Ti powders [19]. The last peak at 30.9 nm^{-1} is the Al(200).

As can be seen in the 3–6 h patterns, there is a peak broadening with a concomitant peak height (intensity) decrease. In particular, a different peak ratio is observed for the 26.9 nm^{-1} reflection, together with the reduction of the Al (200) peak: this result is indicative of a progressive Al diffusion into the Ti lattice.

After milling for 6 h the Al(200) reflection is less clear, suggesting almost complete diffusion of Al into the h.c.p. lattice of α-Ti. Thus, from the 6 h pattern it is possible to envisage a Ti(Al) solid solution, plus some fraction of unreacted TiH_2 and a small quantity of still undissolved Al. At this stage of milling no experimental evidence of an amorphous phase formation is observed, even if the broadened profiles are indicative of a highly fragmented and defective solid solution.

The situation at 16 h reflects a complete diffusion mechanism showing broadened peaks due to further crystallite size reduction together with a concomitant high distortion of the h.c.p. Ti(Al) phase. The peak position corresponding to Ti(010) remains unchanged in this stage, while those corresponding to Ti(002) and Ti(011) move to higher q values, suggesting a contraction mainly of the h.c.p. c parameter.

At higher milling times of 20–24 h an amorphous phase develops, and finally at 34 h a nanocrystalline f.c.c. phase was indexed with a lattice parameter $a = 0.42$ nm.

3.2. Electron microscopy

The details of the microstructural evolution with milling time are best provided by TEM observations. As already observed by scanning electron microscopy (SEM) [16], in the early milling stages (up to 6 h) the powder particles assume a flaked irregular morphology, indicative of a strong cold welding of the elemental crystalline powders.

The analytical electron microscopy (AEM) observations showed that the cold welding results in a bulk stressed layered morphology, clearly evident in the micrograph of Fig. 2. The thickness of the individual layers is approximately 200–300 nm. Electron diffraction and EDS analyses showed both the presence of h.c.p. and f.c.c. phases, and also the presence of zones of pure Ti and Al. In fact, careful observation of the bulk layers, performed at higher magnification (Fig. 3), reveals that they are made of Ti with sublayer zones of Al of various thicknesses (ranging from 15 to 20 nm) inhomogeneously distributed in the Ti matrix. Appreciable Al diffusion into the Ti lattice was also observed.

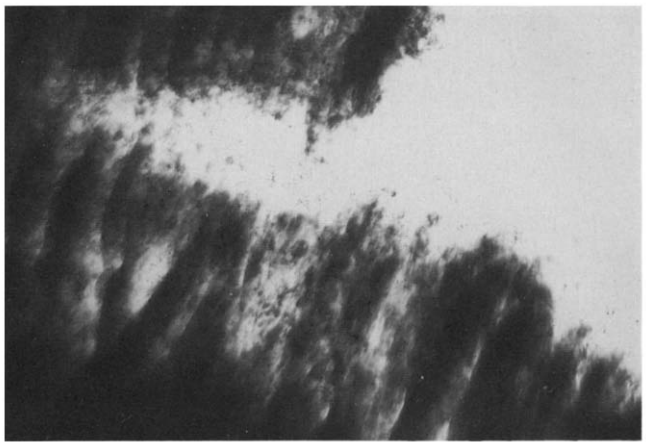

Fig. 2. TEM image of a powder particle ball milled for 6 h. A bulk stressed layered morphology with individual layer thickness approximately 200–300 nm is evident. Lateral field width is 2300 nm.

Fig. 3. Detail of the layered microstructure developed after milling for 6 h. The Al thinner sublayers are inhomogeneously distributed among extended strain contrast. Lateral field width is 400 nm.

A new feature develops after milling for 16 h (Fig. 4). The layered structure is still evident, but the thickness of the layers is strongly reduced to 30–40 nm. The corresponding microdiffraction pattern reveals only the presence of an h.c.p. phase, as shown in the diffraction inset. Several tiny Ti crystals (of a few nm) are also visible among the layers in the micrograph. EDS nanoanalyses performed scanning the electron beam across the layers, clearly demonstrated a profile of Al diffusion into the Ti layers, as evidenced from the sequence of EDS spectra shown in Fig. 5. At this stage the crystallites

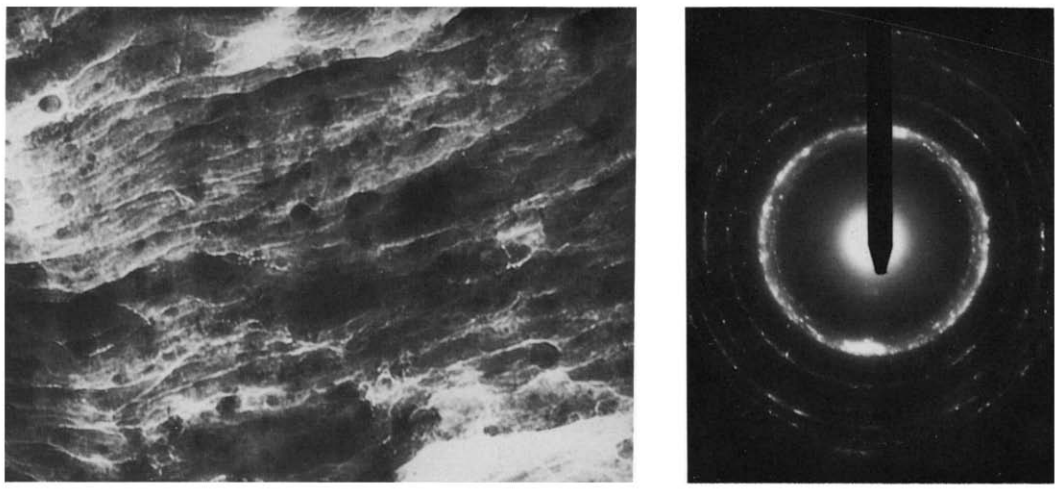

Fig. 4. TEM image of powder particle ball milled for 16 h. Electron diffraction pattern in the inset showing the presence of an h.c.p. phase. Lateral field width is 800 nm.

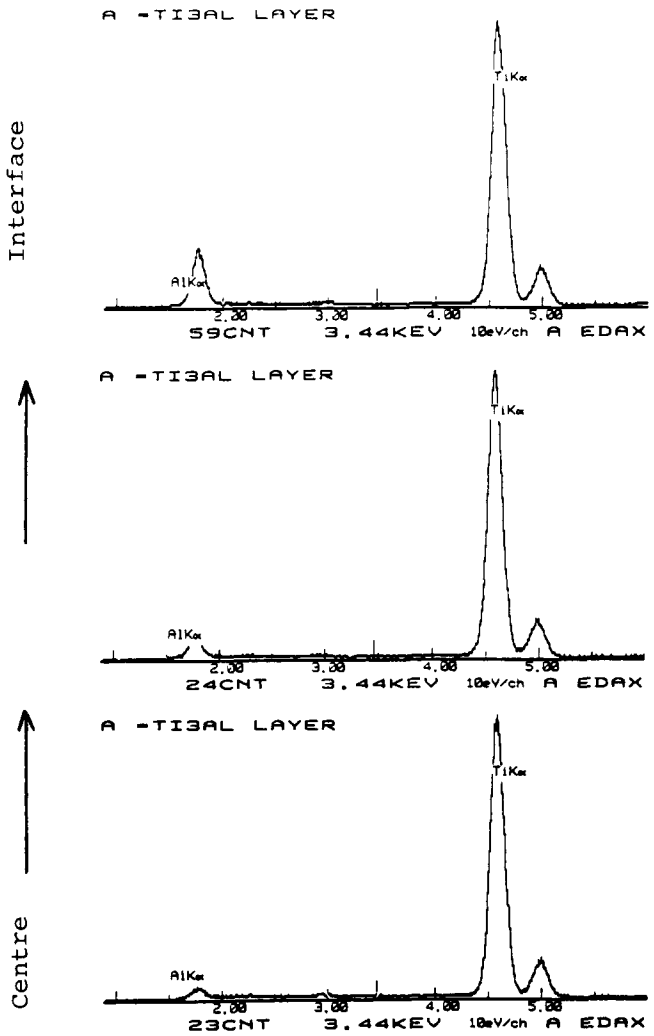

Fig. 5. EDS nanoanalyses performed moving the electron probe from the centre to the interface of a layer of Fig. 4, confirming a gradient of Al diffusion in the Ti lattice. Electron probe size is 5 nm.

are about 10 nm. It is worth noting the persistence of an extended strain distribution among the layers.

After milling for 20 h a layered structure with layers about 30 nm thick is still visible (Fig. 6). The corresponding electron diffraction pattern shows that an incipient long-range amorphization develops, starting from destabilization of the h.c.p. host lattice, in particular in the (002) and (101) reflections, while persistent distorted nanocrystallites remain, about 5 nm in size. PEELS analyses performed to check whether possible oxidation or nitridation had occurred, did not show any presence of oxygen or nitrogen, as can be seen from a typical spectrum reported in Fig. 7.

After milling for 24 h a complete long-range amorphization takes place, as can be seen in the micrograph with the corresponding halo ring shown in the inset of Fig. 8. Other important features are deduced from the AEM observations:

(i) The EDS analyses performed on the amorphous products showed (Fig. 9) that an atomic ratio Ti/Al of approximately 3 is found.

(ii) A latent layered morphology is still observable with "layers" of the same thickness as in the products milled for 16 h, suggesting a critical layer thickness of about 30–40 nm for the stressed Ti(Al) h.c.p. to Ti(3) Al amorphous phase transformation.

(iii) In Fig. 8, very small (less than 5 nm) homogeneously distributed diffracting crystals are also present in the amorphous matrix, probably arising from unreacted Ti or incipient nanocrystallization.

After milling for 34 h a nanocrystalline product is obtained (Fig. 10). The grains are about 5 nm, with a Ti–Al at. ratio of approximately 3, as shown from EDS (Fig. 11). From the corresponding electron diffraction pattern, reported in the inset, a f.c.c. structure can be indexed with a lattice parameter $a = 0.41$ nm,

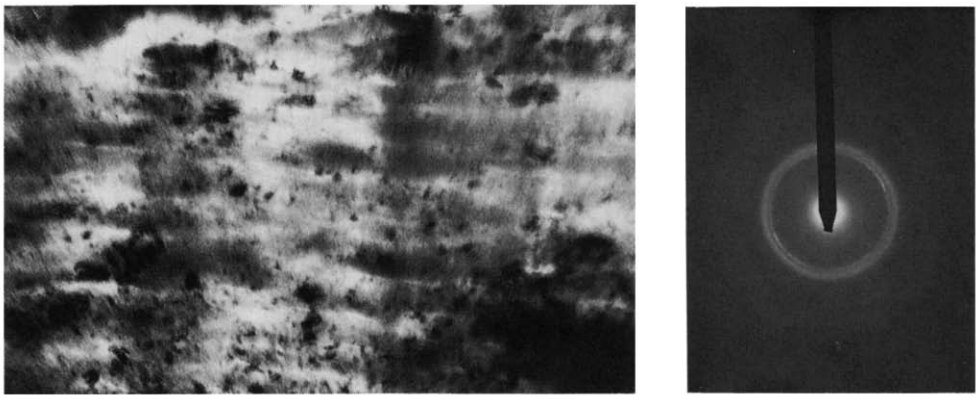

Fig. 6. TEM image of sample milled for 20 h with the corresponding electron diffraction pattern shown in the inset. Lateral field width is 800 nm.

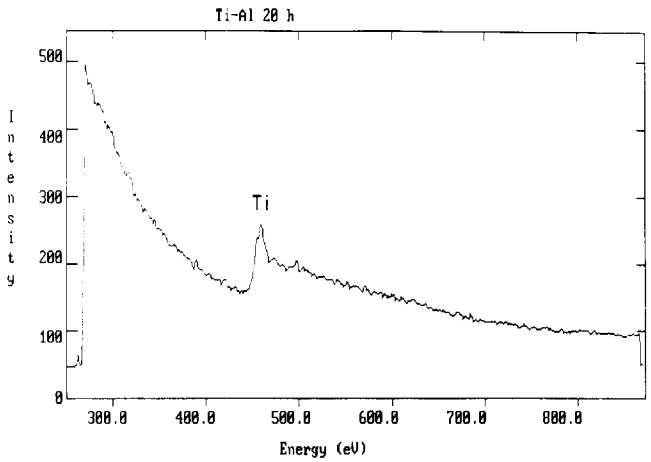

Fig. 7. PEELS analysis of the 20 h sample; no oxygen or nitrogen is detected. The edge is that of Ti L2,3.

in good agreement with the figure of 0.42 nm previously reported from XRD data.

It must be pointed out that PEELS showed the presence of large amount of nitrogen at this stage of milling (Fig. 12). Some particles of WC coming from the vial were also found in the specimens (Fig. 13, arrowed), explaining the XRD peak at $q \sim 25$ nm^{-1} present at this stage of milling.

4. Discussion

The analytical electron microscopy observations of the MA powders have confirmed as previously reported [16] that an amorphization of the milled products takes place after milling for approximately 20 h. The more

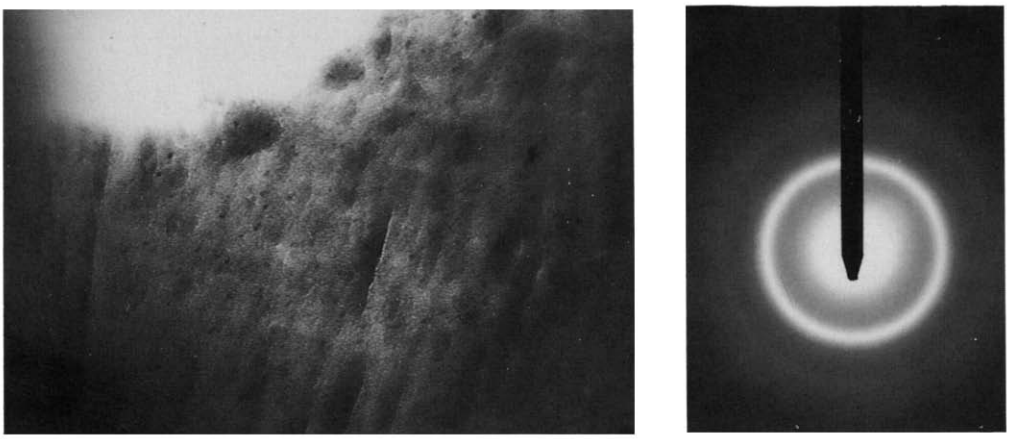

Fig. 8. TEM image of a sample ball milled for 24 h. The corresponding microdiffraction pattern is shown in the inset. Lateral field width 800 nm.

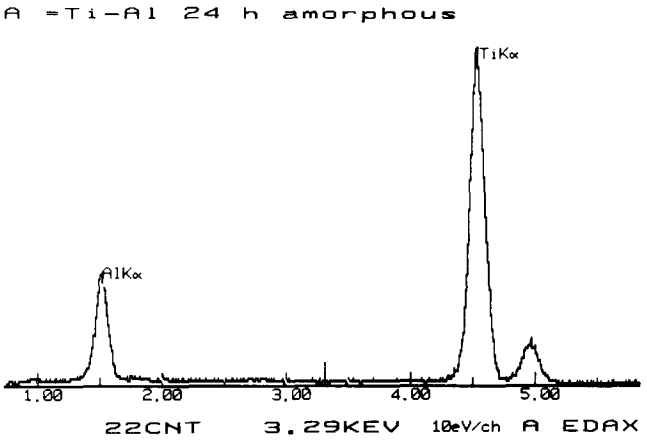

Fig. 9. EDS analyses of a powder particle milled for 24 h. The amorphous phase shows an atomic ratio Ti–Al of approximately 3.

detailed TEM observations coupled with EDS and PEELS analyses performed in the present research offer some hints as to possible amorphization triggering mechanisms. In this respect the following factors are relevant:

(i) the interdiffusion of Al into the Ti lattice;

(ii) the formation of an extended α-Ti(Al) solid solution with a high defect density, and layered morphology;

(iii) finally, the amorphization of the particle layered structure that forms at later stages of milling.

Our results offer no experimental evidence for amorphization occurring, at least locally, by interdiffusion originating in finely comminuted Ti–Al domains, as in some metal–metal multilayered systems such as Ni–Zr [8]. The amorphization, in this case, starts only after a complete Al diffusion into the α-Ti lattice.

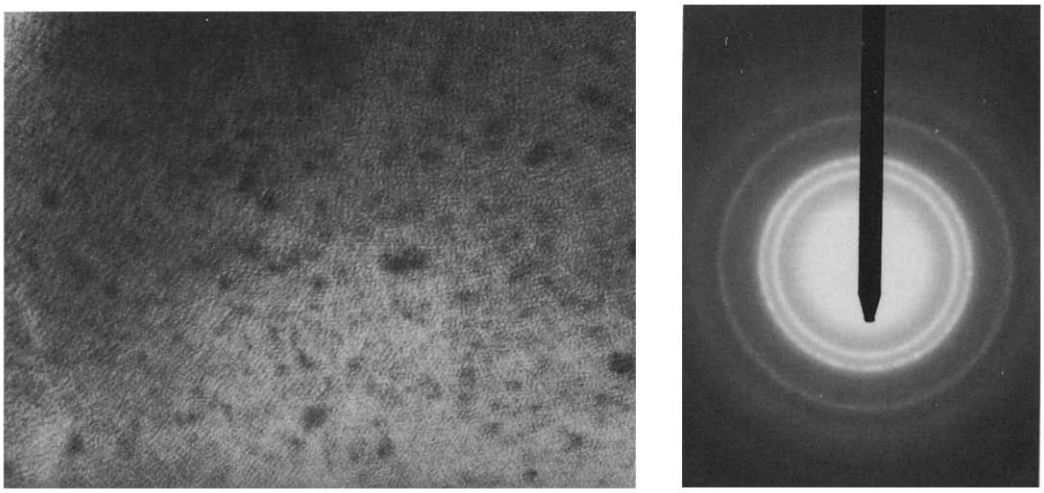

Fig. 10. TEM image of a sample ball milled for 34 h with corresponding electron diffraction pattern. Lateral field width 150 nm.

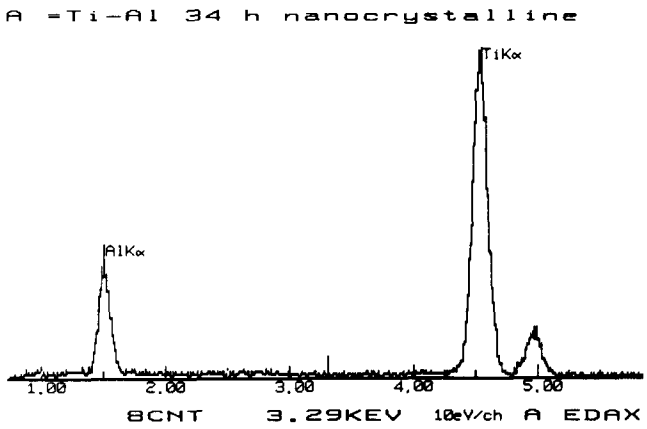

Fig. 11. EDS analysis of 34 h BM sample; Ti–Al at. ratio approximately 3.

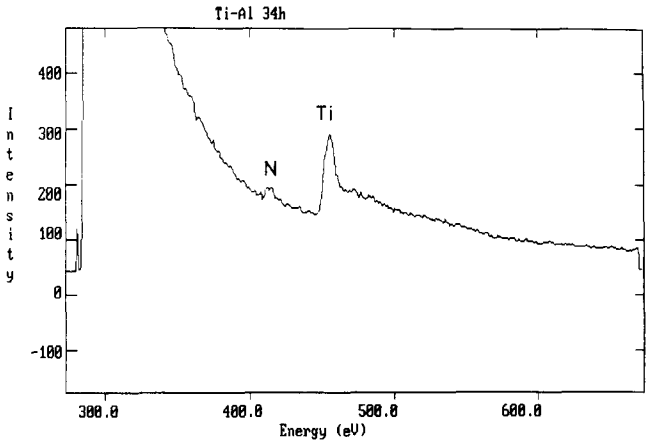

Fig. 12. PEELS of 34 h BM sample; note the presence of large amounts of nitrogen.

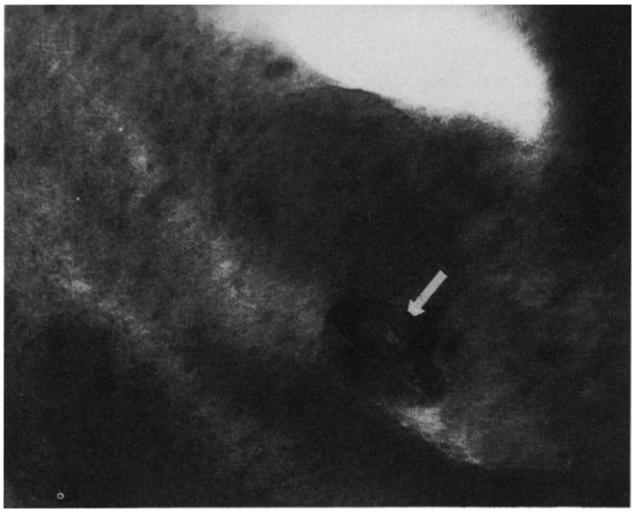

Fig. 13. TEM image showing a WC particle (arrowed) embedded in the 34 h BM sample. Lateral field width 100 nm.

The detailed AEM studies showed that, in our experimental milling conditions, an almost complete dissolution of Al into the α-Ti lattice occurs for milling times greater than 6 h. However, at 6 h we can still notice, as is evident from Fig. 3, some unreacted Al. The two-phase layered structure formed is not homogeneous: the Ti layers approximately 300 nm thick are separated by thinner Al layers about 20 nm thick, irregularly distributed. The corresponding XRD pattern, still shows a faint Al(200) peak discernible from the background.

The presence of diffraction contrast in the TEM images, resulting from strained structures, in agreement with XRD interpretation of line broadening, should also be noted. After 16 h a layered structure made up of 30–40 nm thick layers of Ti(Al) strained h.c.p. phase is shown by electron diffraction (Fig. 4). EDS analyses (Fig. 5) reveal in addition an Al concentration gradient in the α-Ti(Al) layers. Note that XRD shows related lattice parameter changes in agreement with recent observations on the Zr–Al system [12]. Further milling leads to an incipient amorphous phase formation, as can be seen from the micrographs (Fig. 6).

These results, together with the observation of a persistent long-range stressed microstructure, reflecting the occurrence of a highly distorted h.c.p. Ti phase, are consistent with the existence of a stability limit for the high free energy metastable solid solution at the onset of amorphization. It seems that the stressed structure observed reflects a high enthalpy state where a combination of atomic site disorder plus linear and surface defects plays a crucial role, analogous to the amorphization of intermetallics.

Several components of the enthalpy of the system must be envisaged. One is a term linked to the linear or surface defects introduced during ball milling, δH^{def}, this is essentially the sum of two terms δH^{dis} and δH^{gb} that represent the energy stored at dislocations and grain boundaries of the system. Another important contribution is to be expected from the chemical disorder energy δH^{ch} which is established in the h.c.p. Ti(Al) solid solution.

If the enthalpy of crystallization of the amorphous phase δH^{cr} can be evaluated, a sufficient condition for amorphization starting from the homogeneous h.c.p. Ti(Al) solid solution is then expressed by the inequality

$$\delta H^{\mathrm{def}} + \delta H^{\mathrm{ch}} > \delta H^{\mathrm{cr}}$$

Several attempts have been reported in the literature to calculate the amount of stored energy arising from defects $\mathrm{d}H^{\mathrm{def}}$ (lattice strain energy) in metallic systems, but the results are controversial. In pure Ni and Ti metals we have found [17] lattice strain densities of the same level as previously reported figures in cold worked metals [20] (typically 0.1–0.2%), but other authors have reported values one order of magnitude larger [21, 22]. It must be pointed out that the defect content is generally calculated by using the XRD line broadening method of Warren–Averbach [23], which gives a strain distribution over the crystal sizes. There is no clear agreement on where to take the average of the crystal sizes. In addition, some results making use of the alternative Williamson–Hall [24] method have given different outcomes at parity of experimental data. This topic has been critically addressed by Wagner and Boldrick [25]. In any case, what emerges is that the enthalpy stored by lattice strain is of the order of 1–2 kJ mol^{-1}, a value which is insufficient, alone, to account for the amorphization of solid solution and/or intermetallics.

As regards the δH^{ch} term, as experimentally observed (Figs. 4, 5), a strong concentration gradient of the dissolved Al in the Ti lattice is observed in the 16 h milled products, *i.e.* just before transformation to the amorphous phase. This concentration profile can raise the δH^{ch} term locally, as suggested also by Fecht *et al.* in the Zr–Al system [12].

Another factor that can play a decisive role is TiH_2 contamination present in our "pure" Ti powders. For this reason, the role of contaminants in Ti-based alloys, made amorphous by MA, is being studied extensively by neutron diffraction [19]. Because the Ti used in these samples was also TiH_2 contaminated, it is probable that interdiffusion and amorphization are also activated to a certain extent by the presence of a small fraction of these hydrides.

The TiH_2 can act as a catalyst for interdiffusion or can participate in the SSAT by analogy with the amorphization of Rh_3Zr induced by H_2 diffusion [26]. In any case, this effect can be ascribed to both the δH^{ch} and δH^{def} terms, and its effect is currently under investigation.

It may be safe to conclude that the amorphization is triggered from the extended solid solution by the synergistic combination of the terms here described, in the sense that, the presence of one factor can influence the extent of participation of the others. We can exclude the role of oxygen and nitrogen because they were not detected in the pre-amorphization products.

5. Conclusions

Analytical electron microscopy and XRD investigations on MA Ti_{75}–Al_{25} powders have indicated a complete amorphization reaction of the milled products. TEM observations with EDS analyses indicate that the entire transformation process starts when a high energy metastable microstructure is developed in the particles. This is made up of a layered structure of a chemically disordered h.c.p. phase. After this, the amorphization transformation is observed. High resolution transmission electron microscopy observations would be useful for investigating this mechanism in more detail. These results are in any case consistent with models based on amorphization induced by lattice destabilization. However, a contribution may also be expected from hydride contaminants in promoting the transformation.

Acknowledgments

The authors wish to thank Professor L. Battezzati and Professor P. Gaskell for useful discussions and comments. The skilful technical assistance of Mr. R. Berti is also gratefully acknowledged. This work was performed under the INFM National project Metastable Phases and partially supported by Ministero della Ricerca Scientifica e Tecnologica, and MICROMAT, Italy.

References

1 K. C. Russel, *Prog. Mater. Sci., 28* (1984) 229.
D. E. Luzzi, H. Morri, H. Fujita and M. Meshii, *Acta Metall., 34* (1986) 629.
2 B. M. Clemens, W. L. Johnson and R. B. Schwarz, *J. Noncryst. Solids, 61-62* (1984) 817.
3 A. Blatter and M. von Allmen, *Phys. Rev. Lett., 54* (1985) 2103.
4 C. C. Koch, O. B. Cavin, C. G. McKamey and J. O. Scarbrough, *Appl. Phys. Lett., 43* (1983) 1017.
5 R. B. Schwarz, R. P. Petrich and C. K. Saw, *J. Non-Cryst. Solids, 76* (1985) 281.
6 A. Ye. Yermakov, Ye. Ye. Yurchikov and V. A. Barinov, *Phys. Met. Metallogr. (USSR), 52* (1981) 50.
7 R. B. Schwarz and W. L. Johnson, *Phys. Rev. Lett., 51* (1983) 415.
8 L. Schultz, *Mater. Sci. Eng., 97* (1988) 15.
9 E. Hellstern and L. Schultz, *Phil. Mag. B, 56* (1987) 443.
10 R. B. Schwarz and C. C. Koch, *Appl. Phys. Lett., 49* (1986) 146.
11 W. L. Johnson, *Prog. Mater. Sci., 30* (1986) 81.
12 H. J. Fecht, G. Han, Z. Fu and W. L. Johnson, *J. Appl. Phys., 67* (1990) 1744.
13 P. R. Okamoto, L. E. Rehn, J. Pearson, R. Bhadra and M. Grimsditch, *J. Less-Common Met., 140* (1988) 231.
14 C. Massobrio, *Coll. Phys. C4-55* (1990).
15 S. Enzo, E. Bonetti, I. Soletta and G. Cocco, *J. Phys. D., 24* (1991) 209.
16 E. Bonetti, G. Valdré, S. Enzo and G. Cocco, *Mater. Sci. Technol., 6* (1990) 1258.
G. Cocco, I. Soletta, L. Battezzati, M. Baricco, S. Enzo, *Philos. Mag. B, 61* (1990) 473.
17 G. Cocco, S. Enzo, L. Schiffini and L. Battezzati, *Mater. Sci. Eng., 97* (1988) 43.
18 D. McMullan and S. B. Berger, *Inst. Phys. Conf. Ser.,* (1988) 131.
19 P. K. Ivison, N. Cowlam, I. Soletta, G. Cocco, S. Enzo and L. Battezzati, *Mater. Sci. Eng., A134* (1991) 859.
20 H. P. Klug and L. A. Alexander, *X-ray Diffraction Procedures for Polycrystalline and Amorphous Materials*, Wiley, New York, 1974.
21 M. Atzmon, K. Unruh and W. L. Johnson, *J. Appl. Phys., 58* (1985) 3865.
22 E. Hellstern, H. J. Fecht, Z. Fu and W. L. Johnson, *J. Appl. Phys., 65* (1989) 305.
23 B. E. Warren and B. L. Averbach, *J. App. Phys., 23* (1952) 497.
24 G. K. Williamson and W. H. Hall, *Acta Metall., 1* (1953) 22.
25 C. N. J. Wagner and M. S. Boldrick, *Mater. Sci. Eng., A133* (1991) 26.
26 X. L. Yeh, K. Samwer and W. L. Johnson, *Appl. Phys. Lett., 42* (1983) 242.